

# DESIGN AND MODELING OF A KINEMATICALLY-CONSTRAINED TRACTION-DRIVE SPINDLE FOR MICRO MACHINING

Christopher J. Morgan<sup>1</sup>, R. Ryan Vallance<sup>2</sup>, Eric R. Marsh<sup>3</sup>,

<sup>1</sup>Mechanical Engineering, University of Kentucky  
Lexington, KY, USA

<sup>2</sup>Mechanical and Aerospace Engineering, The George Washington University  
Washington, DC, USA

<sup>3</sup>Mechanical and Nuclear Engineering, The Pennsylvania State University  
State College, PA, USA

## INTRODUCTION

Micro machining has become an important technique for fabrication of miniaturized components for automotive, aerospace and biomedical applications [1][2]. Many micro machining areas, such as, micro milling, micro drilling and micro grinding [3] require a cnc machine tool with a high speed spindle. High speed spindles are necessary for increasing cutting speeds with small tools. As researchers strive for more precise micro features and smaller unit removal, the error motion of the spindle [4] and tool runout become critical. Significant improvements in the precision and accuracy of linear positioning stages within machine tools now provide positioning resolutions on the order of a nanometer. However, reductions in the error motion of high-speed spindles remains limited to values on the order of a micrometer. This high dynamic runout causes poor tool life, decreased precision, and increased roughness. Spindles with speeds greater than 200,000 rpm are limited to conventional aerodynamic bearings [5]. These bearings are difficult to balance, which leads to whirling of the rotor [6]. Also, accurate alignment of a tool's centerline with a spindle's axis-of-rotation is challenging with taper and collet tool holders.

Some alternatives to high-speed aerodynamic spindles are under development or available for particular applications. Some of these seek to alleviate the tool holder problem. Pathak [7] used the tool shank directly as the rotor in a porous graphite journal bearing. The tool shank was driven by a traction roller powered by a high speed spindle. Although the spindle achieved speeds in excess of 400,000 rpm, the tool runout was poor due to the error motion of the rotating traction roller. High speed spindles for micro machining continue to be investigated at the University of Florida. Another alternative is used by

IDCT Microdrilling Systems [8]. Instead of placing the tool shank in a bearing, it is pinched between 3 cylindrical rollers. Two of the rollers are powered, and one is an idler. The diameter ratio between the rollers and the tool shank increases the rotational speed. In this configuration, the tool shank wanders slightly in the axial direction, and IDCT utilizes this to actuate the tool axially by skewing the cylindrical rollers. This technology works well for micro drilling, but it is not suited to micro milling or micro grinding since the tool shank should be constrained in the axial direction.

This paper considers a new spindle concept that incorporates a traction drive system that kinematically constrains the position and orientation of the tool. The concept is similar to the kinematic spindle described by Hii *et al.* [9] but with some crucial differences. Here, the spindle's rotor is supported at contact points that are not stationary, and the constraint lines supporting the rotor are oriented so that they intersect at three points. This paper describes the spindle concept, models for the stiffness of the spindle, a model for predicting quasi-static errors, and a method for determining values of design parameters. These models are applied in a case-study for evaluating the concept prior to prototype construction.

## DESIGN

Figure 1 illustrates some details of the kinematically-constrained traction drive spindle. The top view identifies two stationary air bearing spindles and a third air bearing spindle mounted on a single degree-of-freedom flexural bearing. Six spherical rollers form the traction drive and are attached to the top and bottom surfaces of the three air bearing spindles. An additional shaft (toolholder) holds the micro machining tool and acts as the spindle's rotor. It

is pinched between the six traction-drive rollers. A single motor drives one of the stationary air bearing spindles and causes the rotor/toolholder to spint at a multiple of the air bearing spindles' speed.

Each spherical roller contacts a conical surface on the toolholder/rotor at a single contact point. This establishes six constraint lines that intersect the contact points normal to the contact surfaces. These constraints establish the position and orientation of the rotor/toolholder kinematically or in an exact-constraint fashion [10]. The flexure provides a preload force between the traction rollers and the rotor.

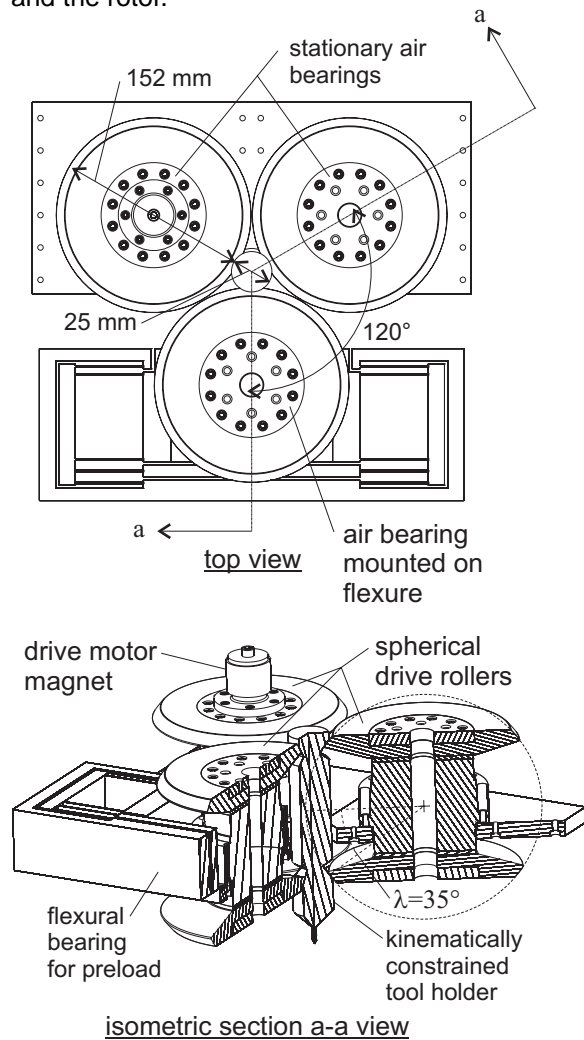


FIGURE 1. Design of a kinematically-constrained traction-drive spindle for micro machining

## SYSTEM MODELING

### Three-Dimensional Model

Figure 2 identifies the location of components within the spindle using a system of vectors and transformations between coordinate systems, the forces applied at the tip of the tool, and the reaction forces at six contact points. The position and coordinate system of bearing #1 serves as the origin of the system. The position vectors of the bearing stators are denoted by  $\overline{S}_i$  where  $i = 1, 2, 3$  represents the bearing number. The variable  $\overline{q}_i$  represents any error between the bearing stators. The variable  $\overline{\alpha}_i$  represents rotation errors that occur between the bearing stators. The positions of the rotors in the air bearing spindles are denoted by  $\overline{B}_i$ . The coordinate systems for the bearing stators and rotors are denoted by  $\{\hat{s}_i\}$  and  $\{\hat{b}_i\}$ . The transformation matrices that locate the bearing stators and rotors may now be determined:

$$\overline{S}_2 = q_{21}\hat{s}_{11} + q_{22}z_1\hat{s}_{12} + q_{23}\hat{s}_{13} \quad (1)$$

$$\overline{S}_3 = q_{31}z_2\hat{s}_{11} + q_{32}z_1/2\hat{s}_{12} + q_{33}\hat{s}_{13} \quad (2)$$

$$\{\hat{s}_i\} = [C_1(\alpha_{i1})][C_2(\alpha_{i2})][C_3(\alpha_{i3})]\{\hat{s}_1\} \quad (3)$$

$$\{\hat{b}_i\} = [C_1(\theta_{i1})][C_2(\theta_{i2})][C_3(\theta_{i3})]\{\hat{s}_i\} \quad (4)$$

$$\overline{b}_i \overline{B}_i = \overline{d}_i + b_i \overline{S}_i \quad (5)$$

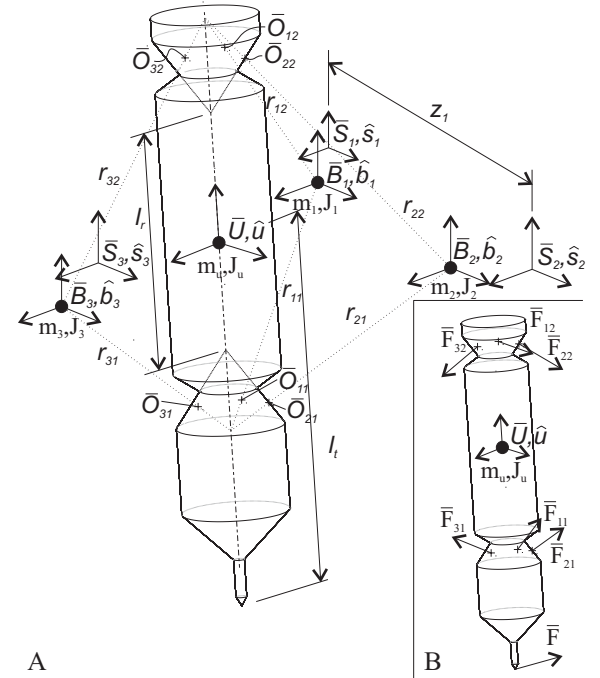


FIGURE 2. A) Diagram detailing geometric relationships of the bearings and tool holder B) Free body diagram of the tool holder with applied forces

where  $[C_1]$ ,  $[C_2]$  and  $[C_3]$  are direction cosine matrices about the 1,2 and 3 directions, respectively. The position of the tool holder is represented by  $\overline{U}$  with the coordinate system  $\hat{u}$ . The contact points are represented by  $\overline{O_{ik}}$ , where  $k = 1$  represents the lower points and  $k = 2$  represents the upper points. The effective radius of each spherical roller is denoted by  $r_{ik}$ , resulting in the following equation:

$$|\overline{O_{ik}B_i}| = r_{ik} \quad (6)$$

The points  $\overline{O_{ik}}$  lie on the conical surfaces of the tool holder and are expressed by the following equations in the  $\hat{u}$  coordinate system as:

$$G_1(\overline{uO_{i1}}) = 0 = {}_uO_{i11}^2 + {}_uO_{i21}^2 - \tan^2(\lambda) ({}_uO_{i31} + l_r/2)^2 \quad (7)$$

$$G_2(\overline{uO_{i2}}) = 0 = {}_uO_{i12}^2 + {}_uO_{i22}^2 - \tan^2(\lambda) ({}_uO_{i32} - l_r/2)^2 \quad (8)$$

where  $l_r$  is the distance between the cone vertices. The vectors  $\overline{{}_uO_{ik}B_i}$  are normal to the to the conical surfaces at points  $\overline{O_{ik}}$ . The orthogonality can be expressed by the following equation:

$$\nabla G_k(\overline{{}_uO_{ik}}) \times \overline{{}_uO_{ik}B_i} = 0 \quad (9)$$

An assumption is made that Hertzian contact points are infinitely stiff. The forces and moments acting on each bearing can be summed and written as follows:

$$\sum_{k=1}^2 \overline{{}_bF_{ik}} - [k_{di}] \overline{{}_d} = m_i \overline{{}_d} \quad (10)$$

$$\sum_{k=1}^2 \overline{{}_bF_{ik}} \times \overline{{}_bO_{ik}B_i} - [k_{\theta i}] \overline{{}_\theta} = J_i \overline{{}_\theta} \quad (11)$$

where  $[k_{di}]$  is the linear stiffness matrix of each bearing,  $[k_{\theta i}]$  is the angular stiffness matrix of each bearing,  $\overline{{}_d}$  is the linear displacement of the bearing rotor, and  $\overline{{}_\theta}$  is the angular displacement of the bearing rotor. The forces and moments acting on the tool holder are:

$$-\sum_{i=1}^3 \sum_{k=1}^2 \overline{{}_uF_{ik}} + \overline{F} = m_u \overline{{}_d} \quad (12)$$

$$-\sum_{i=1}^3 \sum_{k=1}^2 \overline{{}_uF_{ik}} \times \overline{{}_uO_{ik}U} + \overline{T} = J_u \overline{{}_\theta} \quad (13)$$

where  $\overline{{}_d}$  is the linear displacement of the tool holder,  $\overline{{}_\theta}$  is the angular displacement of the tool

holder.  $\overline{F}$  and  $\overline{T}$  are the forces and torques applied by the tool. The 1 and 2 directions of the  $\hat{u}$  coordinate system can be arbitrarily selected, and the forces and moments applied to the tool are in these directions. Therefore, they are chosen to be aligned with the 1 and 2 directions of the reference coordinate system. These direction vectors are found by the following equations:

$$\hat{u}_2 = \hat{u}_3 \times [1 \ 0 \ 0] / |\hat{u}_3 \times [1 \ 0 \ 0]| \quad (14)$$

$$\hat{u}_1 = \hat{u}_2 \times \hat{u}_3 \quad (15)$$

The equations listed above represent a system of 129 equations and the number of unknowns is 135. Therefore, an analytical solution of the tool holder and orientation cannot be found. Instead, a computational least squares optimization approach is used. The inputs to the system are;  $\overline{q_i}$ ,  $\overline{\alpha_i}$ ,  $\lambda$ ,  $r_{i,k}$ ,  $l_r$ ,  $[k_{di}]$ ,  $[k_{\theta i}]$ ,  $\overline{F}$  and  $\overline{T}$ .

### Two-dimensional Model

Although the 3D analysis described above is solvable, its results are complex for optimizing the design parameters of the spindle. To develop design equations, the model is simplified to two dimensions as shown in Fig. 3. The loads and de-

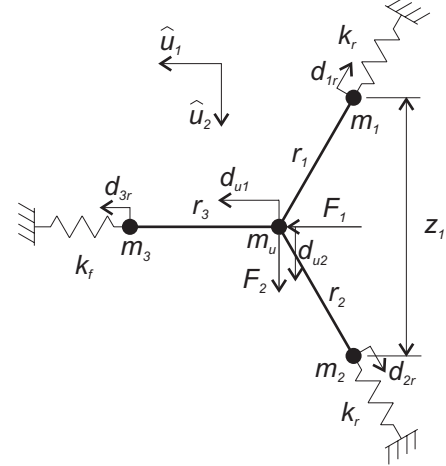


FIGURE 3. Simplified model of spindle kinematics neglecting out-of-plane forces and moments. Flexions in the 3-direction are ignored resulting in a 2D kinematic system. Summing the forces at each mass yields the following equations:

$$m_1 \ddot{d}_{1r} + k_r d_{1r} = -F_{t1} \quad (16)$$

$$m_2 \ddot{d}_{2r} + k_r d_{2r} = -F_{t2} \quad (17)$$

$$m_3 \ddot{d}_{3r} + k_f d_{3r} = -F_{t3} \quad (18)$$

$$m_u \ddot{d}_{u1} - F_{t3} + \frac{1}{2} F_{t1} + \frac{1}{2} F_{t2} = F_1 \quad (19)$$

$$m_u \ddot{d}_{u2} + \frac{\sqrt{3}}{2} F_{t1} - \frac{\sqrt{3}}{2} F_{t2} = F_2 \quad (20)$$

where  $F_{t1}, F_{t2}, F_{t3}$  are the reaction forces at the contacts,  $k_r$  is the radial stiffness of the bearings, and  $k_f$  is the flexural bearing stiffness. Assuming small angle approximations, the displacements  $d_{1r}, d_{2r}$  and  $d_{3r}$  can be related to  $d_{u1}, d_{u2}$  and the change in length of the effective radii,  $q_{1r}, q_{2r}$  and  $q_{3r}$ .

$$\begin{Bmatrix} d_{1r} + q_{1r} \\ d_{2r} + q_{2r} \\ d_{3r} + q_{3r} \end{Bmatrix} = \frac{1}{2} \begin{bmatrix} -1 & -\sqrt{3} \\ -1 & \sqrt{3} \\ 2 & 0 \end{bmatrix} \begin{Bmatrix} d_{u1} \\ d_{u2} \end{Bmatrix} \quad (21)$$

The masses  $m_1, m_2, m_3 = m_i$  because the bearing rotors and spherical rollers are the same size. The flexure stiffness,  $k_f$ , is small to prevent deflections from affecting the preload; therefore, it is negligible. Substituting Eqs. (16)(17)(18) and (21) into Eqs. (19) and (20) yields:

$$\left( m_u + \frac{3}{2}m_i \right) \ddot{d}_{u1} + \frac{1}{2}k_r d_{u1} = F_1 + m_i \ddot{q}_{3r} - \frac{1}{2}k_r (q_{1r} + q_{2r}) - \frac{1}{2}m_i (\ddot{q}_{1r} + \ddot{q}_{2r}) \quad (22)$$

$$\left( m_u + \frac{3}{2}m_i \right) \ddot{d}_{u2} + \frac{3}{2}k_r d_{u2} = F_y + \frac{\sqrt{3}}{2}m_i (\ddot{q}_{2r} - \ddot{q}_{1r}) + \frac{\sqrt{3}}{2}k_r (q_{2r} - q_{1r}) \quad (23)$$

## CASE STUDY

The case shown in Fig. 1 is studied using the 3D and 2D models. The rollers are mounted on high precision air bearing spindles (Professional Instruments, 3R Blockhead®) with the specifications listed in Table 1. Maximizing the size of the rollers results in a reduction ratio of 6:1. Due to the size the bearing, the contact diameter of the rollers and tool holder is chosen as 152 mm and 25 mm, respectively. The maximum speed of the air bearings is 15,000 rpm, therefore the maximum speed of the spindle is 90,000 rpm. The angle,  $\lambda$ , is chosen to be  $35^\circ$  in order to minimize material and size. Therefore, overall diameter of the rollers is  $152/\cos(\lambda)=186$  mm. The flexure stiffness is chosen to be 0.088 N/ $\mu$ m, which is 3 orders of magnitude below the bearing radial stiffness.

### Contact Stiffness

A key assumption in the analytical models is infinite stiffness at the contact points between the spherical rollers and the tool holder. To confirm this assumption, an analysis of the lubrication gap is performed. The contact points will be lubricated with a traction drive oil, Santotrac 50, which allows the contact points to operate in the elasto-hydrodynamic lubrication (EHL) regime, where the lubrication behaves in a Newtonian manner due to high pressure. The Hertzian contact and

TABLE 1. Specifications for Professional Instruments 3R bearing

Parameter	Value
radial stiffness [N/ $\mu$ m]	88
axial stiffness [N/ $\mu$ m]	260
angular stiffness [N-m/ $\mu$ rad]	0.18
rotor weight [N]	14
max rpm	15,000
torque req'd @ max rpm [N-m]	88
max working radial load [N]	140

TABLE 2. Specifications used for the EHL analysis

Lubricant (Santotrac 50)	
$\alpha$ [GPa $^{-1}$ ]	28.7
$\eta$ [Pa-s]	0.0284
solidification pressure [GPa]	1.07
$d\tau/dp$	0.059
Spherical Roller	
radius [mm]	93
E [GPa]	310
$\nu$	0.28
Tool Holder	
radius [mm]	12.5
E [GPa]	220
$\nu$	0.25

hydrodynamic analysis can be modeled as described in [6].

Figure 4 is a plot of the EHL gap and the maximum shear torque versus the applied normal load at the contact points. Silicon nitride and tungsten carbide are chosen as roller and tool holder materials, respectively, due to the high hardness. Elasto-hydrodynamic lubrication is not achieved until the normal load is 66 N, therefore the minimum preload for the spindle is 132 N. This force is just below the maximum operating force of the spindle, 140 N, therefore EHL can be achieved. The change of the bearing gap is minimal over the range of preload forces, therefore the assumption of infinite stiffness is valid. Also, the maximum shear force is sufficient to provide the torque necessary to overcome the torque due to viscous shear in the air bearings.

### Error Budget

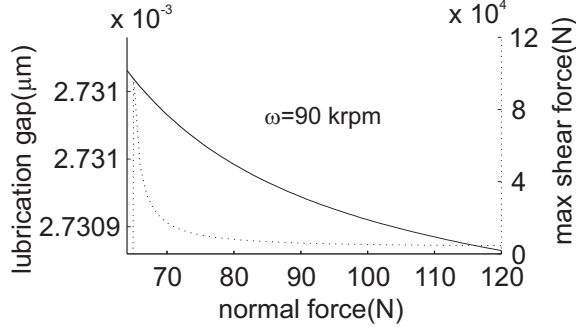


FIGURE 4. Plot of the EHL gap and maximum shear force versus the applied normal load at the Hertzian contacts

Positioning of the bearings is critical to the performance of the EHL contacts. If the spindles' axes-of-rotation are misaligned, the difference in velocity, or slip, is high. The slip ratio is defined as the difference in velocity divided by velocity. Research has shown that slip ratio values above approximately 0.001 can cause the lubricant to behave in a non-Newtonian manner. This causes the EHL analysis to be invalid. The velocity at each of the contact points is calculated to determine the slip ratio.

$$v_{ik} = \omega_i \left| \hat{b}_{i3} \times \overline{O_{ik}B_i} \right| \quad (24)$$

$$v_{uk} = \omega_u \left| \hat{u}_3 \times \overline{O_{ik}U} \right| \quad (25)$$

The bearing degrees of freedom that must be considered are displacements in the  $\hat{b}_{i3}$  direction and rotations about the  $\hat{b}_{i2}$  and  $\hat{b}_{i3}$  directions. Various values of the displacements rotations are applied to the three-dimensional model, assuming quasi-static conditions. The resulting slip is calculated and plotted in Fig. 5. The maximum displacement error occurs when  $q_{23} = -q_{33}$ , and the value is 127  $\mu\text{m}$ . The maximum rotation error occurs when  $\alpha_{21} = \alpha_{22} = -\alpha_{31} = -\alpha_{32}$ , and the value is 1.43 mrad.

### Radial Stiffness

Equations (22) and (23) state that the stiffness of the spindle should be  $0.5k_r$  in the  $\hat{u}_1$  direction and  $1.5k_r$  in the  $\hat{u}_2$  direction. The radial stiffness of the air bearings is 0.5 lb/ $\mu$  in therefore the stiffness of the spindle should be 44 N/ $\mu\text{m}$  in the  $\hat{u}_1$  direction and 132 N/ $\mu\text{m}$  in the  $\hat{u}_2$  direction. Figure 6 is a polar plot the spindle stiffness at various angles in the  $\hat{u}_1 - \hat{u}_2$  plane, solved with the

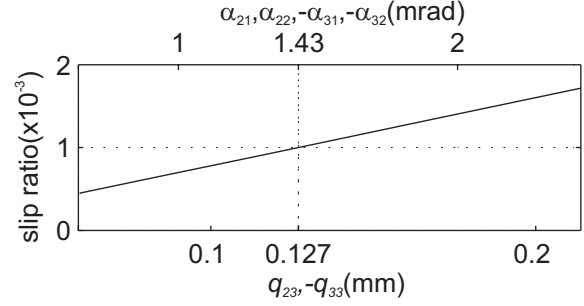


FIGURE 5. Plot of the slip ratio versus linear and angular placement errors of the bearings

three-dimensional model. This plot confirms the stiffness derived with the two-dimensional model.

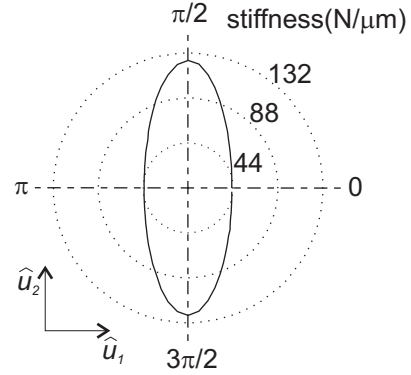


FIGURE 6. Polar plot of the spindle radial stiffness due to loads in the  $\hat{u}_1 - \hat{u}_2$  plane

### Axial Stiffness

The quasi-static analysis is used to generate a plot of the x, y and z deflections of the spindle due to a load in the  $\hat{u}_3$  direction, see Figure 7. The x and y deflections are minimal, and the z deflections follow a slope of 788 N/ $\mu\text{m}$ . The axial stiffness of each air bearing is  $k_z = 1.5 \text{ lb}/\mu$ , and the total axial stiffness of the spindle is simply  $3k_z$ .

### Angular Stiffness

Figure 8 is a plot of the angular stiffness at various angles in the  $\hat{u}_1 - \hat{u}_2$  plane. The stiffness scribes a perfect circle with radius 27.5 lb-in/ $\mu\text{rad}$ . This value is expected due to geometric symmetry of the bearing. If the bearing rotors and tool holder are considered a rigid body, the angular stiffness can be solved by a simple beam with a spring at each end. The following equation expresses that relationship:

$$k_\theta = \frac{3}{2} (r_i + r_u)^2 k_z \quad (26)$$

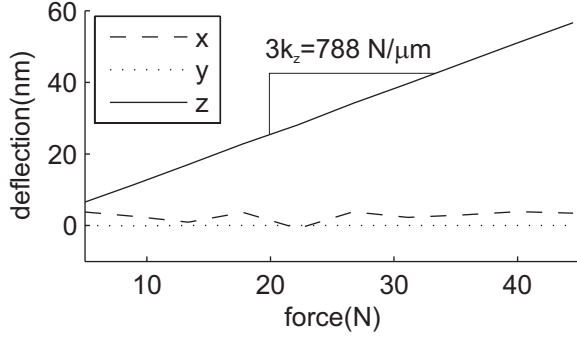


FIGURE 7. Plot of the  $x$ ,  $y$  and  $z$  deflections due to a force in the  $\hat{u}_3$  direction

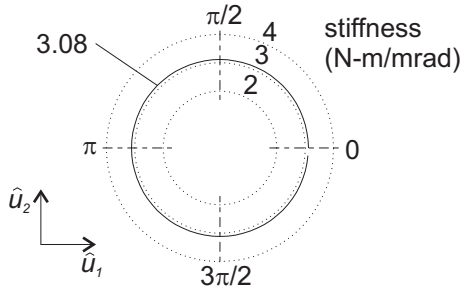


FIGURE 8. Polar plot of the spindle angular stiffness due to loads in the  $x$ - $y$  plane

### Error Motion

Equations 22 and 23 are simple on degree-of-freedom spring-mass equations. Assuming all of the inputs are periodic, the displacements can be expressed as:

$$x = \frac{F_{i1}}{\frac{1}{2}k_r - (m_u + \frac{3}{2}m_i)\omega^2} e^{i\omega t} \quad (27)$$

$$y = \frac{F_{i2}}{\frac{3}{2}k_r - (m_u + \frac{3}{2}m_i)\omega^2} e^{i\omega t} \quad (28)$$

where  $F_{i1}$  and  $F_{i2}$  are the right hand side of Eqs. 22 and 23. The input frequency will depend on the speed of the spindle, as well as the number of undulations per revolution (UPR) on the surface of the spherical rollers and tool holder.

### SUMMARY AND FUTURE WORK

This paper developed models which can be used to find the position a rotating tool holder held within a kinematically-constrained traction-drive spindle for various force and displacement inputs. The results suggest that the spindle would exhibit high stiffness and high speed. Several design challenges remain to be addressed, such as the

removal of the tool holder from the spindle and application of the traction oil.

### ACKNOWLEDGMENTS

This work was partially supported by the Department of Educations GAANN Fellowship, CFD number: 84.200.

### REFERENCES

- [1] Je T, Lee J, Choi D, Lee E, Shin B. Development of a Micro Machining Technology for Fabrication of Micro Parts. *Key Engineering Materials*. 2003;238-239:383–388.
- [2] Murali M, Yeo SH. Rapid Biocompatible Micro Device Fabrication by Micro Electro-Discharge Machining. *Biomedical Microdevices*. 2004;6(1):41–45.
- [3] Masuzawa T. State of the Art in Micromachining. *Annals of the CIRP*. 2000;49(2):473–488.
- [4] ANSI/ASME B89.3.4M. Axes of Rotation: Methods for Specifying and Testing. New York: American National Standards Institute; American Society of Mechanical Engineers; 1985.
- [5] Xichun Luo DW Kai Cheng, Wardle F. Design of ultraprecision machine tools with applications to manufacture of miniature and micro components. *Journal of Materials Processing Technology*. 2005;167:515–528.
- [6] van Beek A. Advanced engineering design: Lifetime performance and reliability. Tu Delft; 2006.
- [7] Pathak JP. Design, Assembly, and Testing of an Ultra-High-Speed Micro-Milling Spindle. University of Florida; 2003.
- [8] IDCT Microdrilling System IDCT. 3100 Fujita Street, Torrance, CA 90505;.
- [9] Hii KF, Vallance RR, Grejda RD, Marsh ER. Error motion of a kinematic spindle. *Precision Engineering*. 2004;28:204217.
- [10] Blanding DL. Exact Constraint: Machine Design using Kinematic Principles. American Society of Mechanical Engineers; 1999.